Journal of Solid Mechanics Vol. 8, No. 2 (2016) pp. 315-325

Analysis of the Fracture of a Turbine Blade

A.R. Shourangiz Haghighi [1], S.Rahmanian [1] , A. Shamsabadi [2, *] , A. zare [3], I. Zare [2]

[1]*Department of Mechanical Engineering, Jahrom University, Jahrom, Iran*
[2]*College of Engineering, Shiraz Branch, Islamic Azad University, Shiraz, Iran*
[3]*Department of Mechanical Engineering, Shiraz University, Shiraz, Iran*

Received 18 February 2016; accepted 5 April 2016

ABSTRACT

The cause of crack initiation turbine blade had initially cracked by a fatigue mechanism over a period of time and then fractured by the overload at the last moment. Experimental procedure consists of macroscopic inspection, material verification, microscopic examination, and metallographic analysis and finally FE. And for these procedures, some specimens were prepared from a fractured blade. Using ICP and energy dispersive X-ray fluorescence, the chemical composition of the blade was carefully analyzed. The segregated area of Ti and Mo, caused generally by inappropriate manufacturing process, is found by the microstructure and EDX analysis of the blade. The fracture blade which installed on the third stage rotor of the turbojet was fractured at about 6 cm distance from the hub of proposed blade. The non-linear finite element method (FEM) was utilized in order to define the stress state of the disc or blade segment under operating conditions. High stress zones were found at the region of the lower fir-tree slot, where the failure occurred. A computation were also achieved with excessive rotational speed. The aim of this study is devoted to the mechanisms of damage of the turbine disc, and furthermore the critical high stress areas.

Keywords : Fatigue; Creep; Turbine blade; FEA; Fracture; X-ray fluorescence.

1 INTRODUCTION

THE fracture on a turbine blade of a turbojet engine has been investigated to see the cause of failure and the crack initiation. The turbojet engine was damaged seriously with loud noise and vibration during flight. Finally the flight was declared an emergency landing uneventfully. The joint between the turbine blade and the disc usually represents the most critical area from the point of view of the static and fatigue approaches. The loads associated with these regions are mainly the centrifugal forces and thermal stresses [1].

The failure and stress analysis of the turbojet engine turbine has received the attention of several investigations. The main problem of numerical estimation of stress state in the dovetail-rim area of disc and blade is completely described by Chan et al. [2], Masataka [3], Meguid et al. [4], Papanikos et al. [5] and Zboinski [6]. Of interest is also work by McEvily [7], Hou [8] described the experimental and numerical investigation of the phenomena happening in the fatigue fracture of turbine blades. Using non-linear finite element analysis, we detailed the phases of the fatigue process. The problem of fatigue fracture of turbine components was defined by Bhaumik [9] and Park et al. [10].

*Corresponding author. Tel.: +98 917 100 2429; Fax: +98 711 3232 1126.
E-mail address: alishamsabadi@ymail.com (A. Shamsabadi).

The use of Finite Element Analysis has long become a common practice during the product development process, especially in the aerospace industry, where a large number of FE codes, including commercial packages and in-house codes are currently in use. The capability covers stress analysis, thermal and vibration analysis, as well as fatigue life estimates. Although most of these tools have user-friendly interfaces and powerful pre- and post-processing capabilities, the successful use of such tools requires experience in the field. These tools are now used at all stages of the design process from concept to detailed design.

During the in-field research, we found that several blades were damaged without fracture and merely one blade was fractured that was installed on the third stage rotor of the turbine as can be seen in Fig. 1.The blade was fractured at about the 6 cm distance from the hub of the blade. And it did not seem to have suffered any damages by any foreign objects because there were no damage on the compressor segment and the first and second stage of the turbine [12, 44].

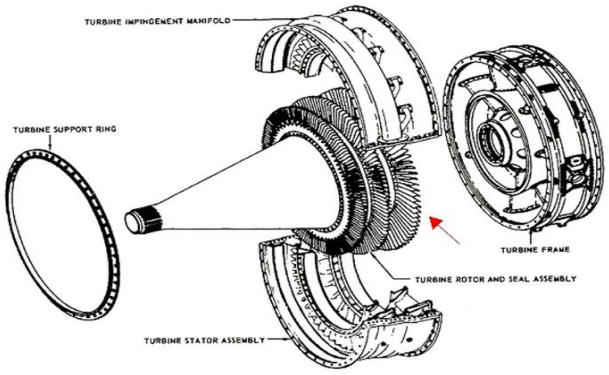

Fig.1
Schematic illustration of the turbine section of the turbojet engine [11, 12]. Note: The arrow indicates the location of the blade failure.

And the rest of paper is organized as follows:

Section 2 deeply proposed the properties of super-alloys which used in turbine blades. As is evident, super-alloys constitute a large fraction of the materials of construction in turbine engines because of their unique combination of physical and mechanical properties. In this section we talk about creep properties such as, Low , intermediate, and High-Temperature Creep.

Section 3 proposed the cause of failure and the important subject crack initiation the fractured blade is sampled and analyzed using a field emission scanning electron microscope (FE-SEM), and a confocal laser scanning microscope ,FEA, etc. [42].

In section 4, we use Finite element model of the third stage turbine disc and the blade, and next Loads, boundary conditions and material properties for FE model investigated.

In section 5, we clearly show the results of the finite element calculations. In this section Von Mises theory is used for calculating stresses in 6 sections. The concluding remarks are presented in section 6.

2 PROPERTIES OF SUPER-ALLOYS

Super-alloys constitute a large fraction of the materials of construction in turbine engines because of their unique combination of mechanical and physical properties. Table 1. lists some typical physical properties of super-alloys. In aircraft engines, it is typical to consider density-normalized properties; therefore alloy densities, which are normally in the range of 7.7–9.0 g/cm^3, are of specific interest.

Table 1
Typical physical properties of super-alloys.[13,15]

Property	Typical ranges
Density	7.7–9.0 g/cm^3
Melting temperature (liquidus)	1320–1450^{0}C
Elastic modulus	Room temp: 210 GPa ,800^{0}C: 160 GPa
Thermal expansion	8–18×10^{-6}/^{0}C
Thermal conductivity	Room temp: 11 W/m ·K, 800^{0}C: 22 W/m·K

Optimization of the relevant set of mechanical properties is of paramount significance and is dependent on a high level of control and understanding of the processes since mechanical properties are a strong function of microstructure. Mechanical properties of primary interest comprise of tensile properties, fatigue, creep, and cyclic crack growth. Depending on the details of component design, each one of these four properties may be life limiting. It is worth noting that models for prediction of these properties must treat many aspects of microstructure at different length scales. For this reason, predictive models for each of these properties now remain under development although in recent years there has been increased effort aimed at property modeling [13].

2.1 Creep properties

Since super-alloys experience extended periods under stress at high temperature, a high resistance to time-dependent creep deformation is crucial. This is significant for cast blade alloys because they will experience temperatures up to 1110^0C, while disk alloys are normally limited to less than 700^0C. For a fixed stress and temperature, two-phase super-alloys have a much higher creep resistance compared to their single-phase counterparts (Fig. 2). As with all properties that governed by plastic deformation processes, creep properties are sensitive to microstructure. The creep-rupture life as a function of volume fraction of precipitates for a single crystal alloy is shown in Fig.3 [14]. Note that the strength peaks when the precipitate volume fractions are in the range of 0.6–0.7. Many alloys contain volume fractions of precipitates in this peak range.

Because the rate-controlling processes in creep are diffusion controlled, elements have low interdiffusion coefficients with nickel are generally beneficial to creep. Interdiffusion for various alloying elements in nickel has been studied in detail [15,16].

Elements most effective at slowing diffusion include Ir, Re, Ru, Pt, W, Rh, and Mo. Advanced creep-resistant alloys benefit from substantial additions of Re, W, and Mo [13,17]. A combination of increasing refractory alloying additions and advances in processing has resulted in substantial increases in the maximum temperature capability of super-alloys over the past few decades. For example, considering a creep-rupture life of 1000 *h* at a stress of 139 MPa, the most developed single-crystal super-alloys have a temperature capability of about 1110^0C, [17] while conventionally cast equiaxed alloys developed in the 1970s had a temperature capability of 900–950^0C [18].

The temperature capabilities have reached 85–90% of the melting point, and frequently high fraction of melting, compared to the operating conditions of any other class of structural materials. This shows a requirement for development of a completely novel class of materials with higher melting points.

The exceptional creep properties are largely as the high resistance of the precipitates to shearing extends to elevated temperatures. The uniaxial stress σ_{0R} needed so as to glide a dislocation through the narrow matrix channels of the super-alloys microstructure is: $\sigma_{0R} = \sqrt{\frac{2}{3}}(\mu b / hS$, where μ is the shear modulus, *b* is the Burgers vector, *h* is the width of the channel, and *S* is the Schmid factor. Typical values of these material properties at 850^0C are $\mu = 48.2Gpa, b = 0.254nm$, and $h = 60nm$ (constant). [19] For these parameters, an applied stress of 408 MPa must exceeded for the onset of dislocation glide through the channels at 850^0C. Hence, its resistance accounts for a large fraction, although not all, of the creep resistance of the two-phase material.

There have been recent efforts in order to model the creep behavior of super-alloys with the use of continuum damage-mechanics methods [20]; however, formulating models which capture the essence of the wide array of complex deformation mechanisms still remains a challenge. The details of the deformation processes are so sensitive to temperature and applied stress, and it is most convenient to consider mechanisms of creep deformation at low, intermediate, and high temperatures [21].

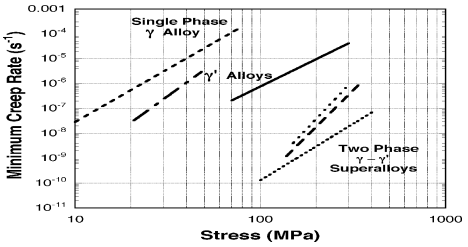

Fig.2
As reflected by the minimum creep rates, two-phase γ–γ' super-alloys exhibit significantly improved creep resistance when compared to their single-phase constituents.

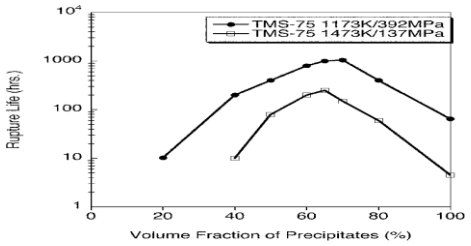

Fig.3
Variation in creep rupture life as a function of γ' volume fraction for single crystal TMS-75 ([14]).

2.2 Low-temperature creep

Super-alloys are so resistant to creep deformation at temperatures below 800^0C. In general creep deformation happens by deformation on (110) {111} slip systems, with an initial preference for dislocation glide through the continuous matrix. Though, at temperatures $<0.6T_M$, high uniaxial stresses might result in the activation of (112) {111} slip systems [24, 45]. When dislocations accumulate at the $\gamma-\gamma'$ interface, 1/2 (110) dislocations undergo reactions that result in (112)-type dislocations that can penetrate into the γ' precipitate. The details of the dislocation reactions that result in such precipitate-shearing processes remain under investigation.[25] Nonetheless, when this shearing process happens , strain is accumulated quickly as a result of the planar nature of the slip and can outcome in high strains during the primary creep transient. This mode of deformation is observed in both polycrystalline and also single-crystal alloys during creep .For instance, in single crystals,[110]-and[111]-oriented crystals are less prone to this type of deformation, while in [13]crystals, planar slip along (112) continues till crystal rotations allow the resolved shear stresses in order to activate slip on other planes. Other factors which influence these shearing processes contain alloy composition, γ size, and volume fraction.

2.3 Intermediate-temperature creep

In this section, stress levels are usually insufficient to result in shearing of the γ' precipitates. Hence, deformation within the microstructure is normally confined to the γ matrix and results in unusual creep curves that contain an initial incubation period and an ephemeral primary transient, followed by an extended period of accelerating creep [26, 27, and 40]. Unfortunately, the steady-state creep rate is not achieved yet.

During the incubation period, no macroscopic straining occurs in part because of the low density of grown-in dislocations. These initial dislocations serve as sources from which dislocations in the γ matrix can easily multiply. In single-crystal experiments, we observed that when an external uniaxial stress is applied, the misfit stresses between the γ' precipitate and γ matrix are unbalanced and the effective stresses enable preferential flow of dislocations within the horizontal channels [48]. The incubation period finishes when dislocation percolation, through the horizontal matrix channels and later through the vertical matrix channels, is complete. The deformation mechanism associated with the primary creep transient during intermediate-temperature creep is clearly dissimilar from that of low-temperature creep. Unlike dislocation shearing of the γ' precipitates along the (112) direction at high stresses and low temperatures, the primary creep transient at intermediate temperatures can be attributed to the relief of coherency stresses at the $\gamma-\gamma'$ interface as dislocations accumulate. At the end of primary creep, a three-dimensional network of dislocations is formed around the precipitates. Despite the lack of a steady-state strain rate, these dislocation networks surrounding the precipitates are stable and contribute to the gradual progression into tertiary creep [27, 28].

2.4 High-temperature creep

The improved diffusivity associated with deformation at extremely high temperatures results in morphological changes within the microstructure [29]. With the application of an external stress to alloys with very important precipitate-matrix misfit, the discrete cuboidal γ' precipitates coalescence into rods or rafts aligned vertical or parallel to the applied-stress direction. The kinetic soft his directional coarsening process are strongly influenced by

the temperature and the stresses associated with the coherency strains at the $\gamma - \gamma'$ interface [25, 30]. Alignment of the rods or rafts, but, is dependent upon whether the external and misfit stresses are tensile or compressive. For instance, uniaxial tensile stresses cause alloys with negative misfit to form rafts perpendicular to the applied-stress direction, whereas compressive stresses applied to the same alloy could result in the formation of rods aligned parallel to the direction of applied stress. Since most commercial directionally solidified and single-crystal alloys clarifies a negative misfit and are used to sustain tensile loads, rafts are formed vertical to the applied-stress direction (Fig. 4).

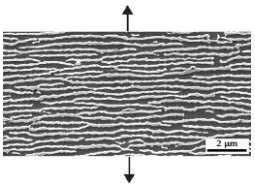

Fig.4
Directional coarsening at elevated temperatures results in the formation of γ rafts aligned perpendicular to the direction of the applied stress. The matrix inverts as the γ rafts are contained within a γ' matrix.

3 EXPERIMENTAL PROCEDURE AND RESULTS

3.1 Material verification of blade

The chemical composition analysis, using ICP and energy dispersive X-ray fluorescence, demonstrates that the blade material is often Nickel alloy M-252 or AMS-5757[22] or E1-867[1]. E1-867 is a precipitation-hardened nickel base alloy, with better creep-resistance for high temperature [1, 12]. The analysis proposed in this paper is performed for elastic–plastic disc and blade materials, with isotropic hardening.

The quantitative chemical compositions of alloy AMS5757 and M-252 are presented in Table 2.[12] for comparison. The measured composition seems to be in agreement with the nominal composition of the Ni-base super-alloys. Ni-base super-alloys were first presented to the aero engines as turbine disc materials so as to allow turbine temperature and stresses to be raised [23]. Note that using Ni-base alloys significantly enable higher fuel efficiency and thrust-to-weight [27].

Table 2
Chemical composition of the blade (wt. %).

	Ni	Cr	Co	Mo	W	Nb	Al	Ti	Mn	Si	Fe	B
Spec M252	55.0	20.0	20.0	20.0	20.0	–	1.00	1.00	0.50	0.50	–	–
Spec AMS 5757c	54.0	19.0	10.0	10.0	–	–	1.00	2.60	–	–	–	0.006
Measured	54.95	18.29	8.96	9.01	0.05	0.08	1.00	2.50	0.01	0.13	0.83	–

Many alloys contain up to 40wt% of a combination of five to ten other elements. As it can be seen in Fig.5(a), the elements normally alloyed with Nickel in order to form a super-alloy are highlighted.
Fig. 5(b) clarifies a typical two-phase $\gamma - \gamma'$ microstructure for a single-crystal turbine-blade alloy. Generally, refractory alloying elements with large differences in electronic structure and atomic radii compared to Ni (for example Mo, W, Re, and Nb) are added for solid-solution strengthening of the γ phase.

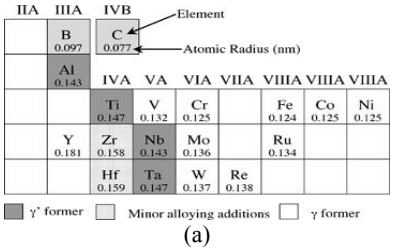

(a)

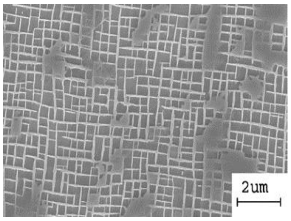

(b)

Fig.5
Alloying elements present in Ni-based super-alloys (adapted from Ref. 2).Microstructure of a Ni-based super-alloy single crystal revealing a high volume fraction of γ' precipitates, which have a cuboidal morphology (courtesy of L. Rowland).

3.2 Microscopic examination

The origin of fatigue is so clear and at the convex area of airfoil (see Fig.6). The figure also clearly demonstrates that the blade fractured rapidly after the progress of the fatigue crack up to 72% of the cross section area.

In order to examine the fractured surface in detail FE-SEM was used. As presented in Fig. 7, tiny striations and dimples are present. As the striations are frequently observed on the fatigue-cracked surface and dimples on

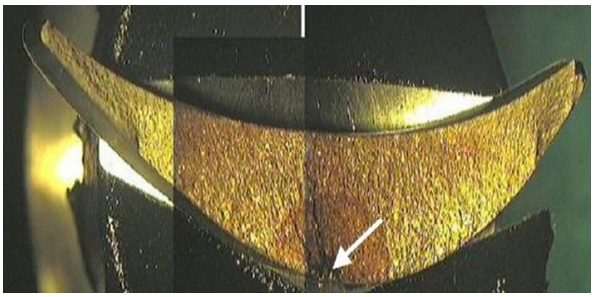

Fig.6
Overview of the fractured surface and the crack initiation site by stereoscope.

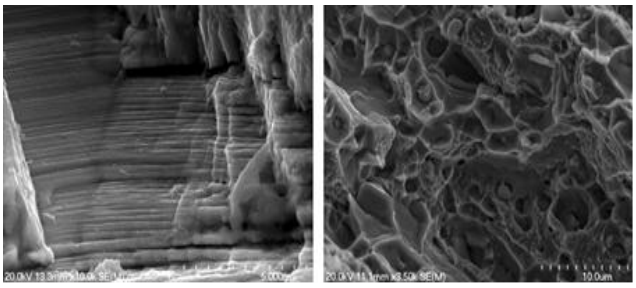

Fig.7
FE-SEM inspection of fractured blade: (a) striations and (b) dimples.

The instant-fractured surface as well, we can strongly conclude that blade had an experience of high cycle fatigue (HCF) from the small striations. HCF failures are unusual in the rotating part of turbine engine, unless some FOD initiates by the ingested debris or a manufacturing fault is present [31, 47].

The FE-SEM fractograph of the crack initiation site, as presented in Fig. 8, shows a feature of the cleavage-like fracture. Generally, cleavage-like fracture is often observed on high-cycle, low stress fracture but unusual in low-cycle, high stress fatigue [22, 31, 32]. In stage II (region B) fatigue, crack marks such as fatigue striations may be appeared.

The schematic plot of fatigue crack propagation rate is shown in Fig. 9. It shows, in detail, that region *A* is mostly influenced by environment, microstructure and mean stress. It was shown by Mercer for Ni-based super-alloys that the mechanisms of fatigue crack growth had a different range of DK for the crack-tip intensity factor [33, 43]. At higher portion of the Paris regime, fracture mechanism transfers to a striated mode. It was similarly reported by Luo and Bowen that the fracture surface is faceted at the lower DK levels while striated at higher DK levels [12, 34]. The phenomena of fractured blade, which have cleavage-like fracture (region *A*), striations (region *B*), and dimples (region *C*) in stages, are fitted with above theory and it is a good sign for us.

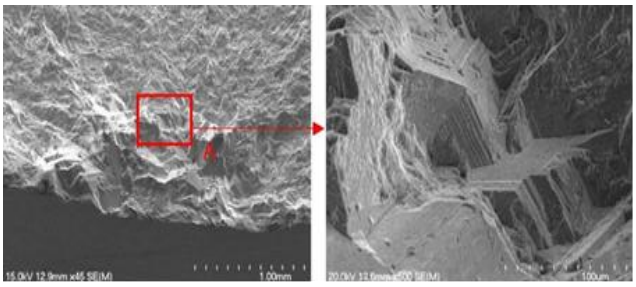

Fig.8
FE-SEM fractographs of a fractured blade: (a) overview of the crack initiation site and (b) cleavage-like fracture (magnified region A).

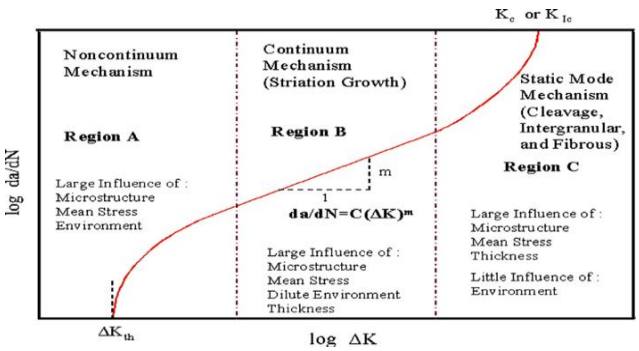

Fig.9
Schematic plot of fatigue crack propagation rate [1, 12].

3.3 Metallography analysis

The microstructures of the blade fractured and the normal blade, as presented in Figs. 10(a), 10(b), are taken from a confocal laser scanning microscopy. It is shown clearly that different sizes of shape, black colored, are concentrated on the edge of blade where the fatigue crack initiated. Also, the grain size of the failed blade is larger than that of the normal blade and the grain has a distribution of various sizes. The microstructure shown in Fig. 8(a) usually appears in the part that is treated by the improper manufacturing process.

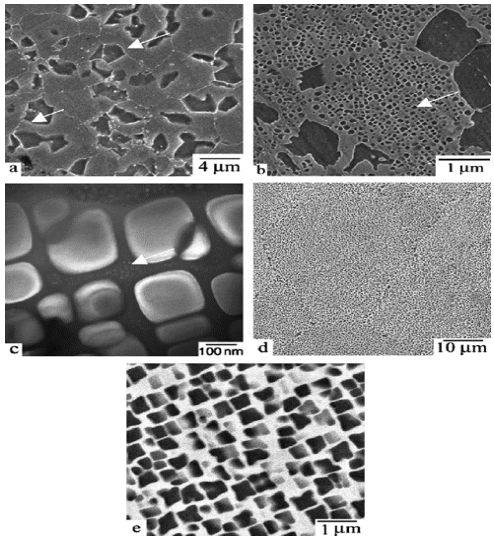

(a)

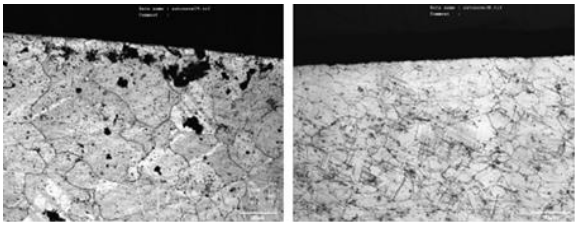

(b)

Fig.10
a) Microstructure of subsolvus and supersolvus processed. b) Microstructure of blade: (a) fractured blade and (b) normal blade.

Using a FE-SEM, EDX analysis in this area has performed and indicated that lumps are composed largely of Ti and Mo as presented in Fig.11(a).The analysis of the normal part, also, shows that its component is consistent with the base material and matches well with its compositions as indicated in Fig.11(b). So it is reasonable to assume that the components of Ti and Mo were formed into segregation at the voids by the unknown reason and then the segregations of Ti and Mo were removed leaving the voids behind during the polishing process. Due to the stress concentration on the segregations near the blade surface, crack is initiated. And this crack begins to progress, then results in an instant-fracture of the overall section.

Generally, the fatigue crack initiates at the surface of specimen as a result of the irreversible process of extrusion or intrusion formation through slip deformation. But some alloys like Titanium alloy or stainless steel change their crack initiation from the surface to the subsurface where it undergoes high cycle fatigue subjected to either a low peak stress or long fatigue life [35, 46].

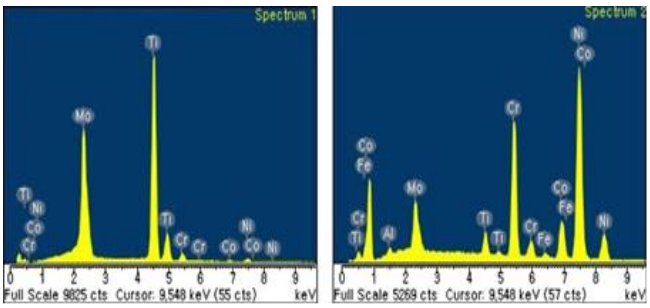

(a) (b)

Fig.11
Micro-chemical analysis of different location by EDX: (a) segregation area and (b) normal area.

Also, the origins of internal fatigue in some materials were attributed to the presence of inclusions [36]. Boyd-Lee showed that crack initiation occurred either within mode II slip bands or within brittle Titanium carbides in the Ni-base super-alloys. Also, he showed that the latter is much easier than the former [37,38]. At the fractured blade, crack initiated at the subsurface or close the surface because of the segregation showing that Ti and Mo segregations act like inclusions.

4 FINITE ELEMENT MODEL OF THE THIRD STAGE TURBINE DISC AND THE BLADE

Parametric geometry models of disc and blade were made, using the MSC-Patran 2009 program. The FE model of disc is shown in Fig. 12(a) which consists of 11,220 nodes and 10,360 first-order HEX-8 elements.

Note that the discretized model of the blade, is shown in Fig. 12(b) consists of 11,430 nodes, 22,248 first-order HEX-8 elements.

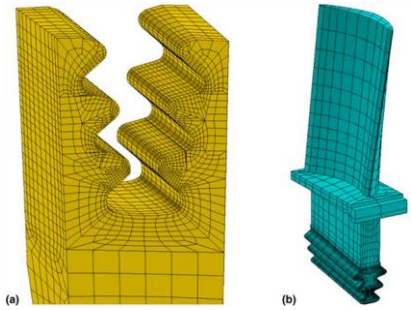

Fig.12
Finite element models of the disc segment (a) and blade (b).

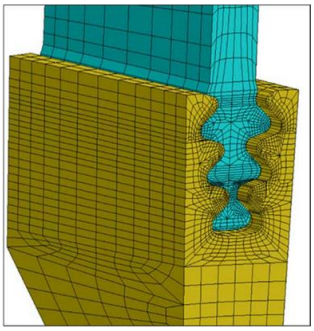

Fig.13
Assembled model of the disc/blade segment in the vicinity of fir-tree slots.

In order to model the mechanical interface of nearby surfaces of the disc or blade, the ‘‘master-slave’’ type of contact with friction coefficient of 0.15 was well-defined for analysis [38,39]. As it can be seen, Fig.13 clarifies the assembled model of the disc or blade section.

4.1 Loads, boundary conditions and material properties for FE model

A rotating hot section component in a turbine engine is in general subjected to a combination of aerodynamic loads, thermal loads, and centrifugal loads. The surface loads are associated with aerodynamic forces [40]. The centrifugal loads arising from the mass of the rotated disc and blades which are generally the most critical loads acting on a turbine disc. Then, this load was easily determined through finite element calculation (after defining the axis of symmetry). In this work, the operational turbine speed of 12,500 rpm was applied. Furthermore, the computation for the rotational speed range of 0–23,000 rpm were made so as to analyze the phenomena which occurring in the turbine during extreme speed. Fig.14 clearly shows the simplified thermal load in Celsius scale.

The turbine disc is usually manufactured out of H-46 material [22, 38]. These properties along with good weld ability and formability account for its wide use in aerospace applications. The yield point of H-46 alloy is equal to 921 MPa, and the UTS is 1200 MPa [39].

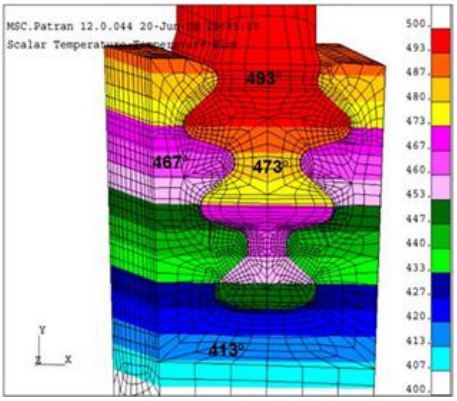

Fig.14
Thermal field defined for models of disc and blade in the dovetail-rim region.

5 RESULTS OF THE FINITE ELEMENT CALCULATION

For all results, Mega Pascal (MPa) units is used in order to describe the stress.The additional aim of this work was to indicate the critical areas with excessive rotational speed. For this purpose, in the numerical model the following characteristic points, shown in Fig. 15 as follows:

(1) Top part of the blade,
(2) Bottom part of the blade (connection between fir-tree slots and blade),
(3) Outside corner of the disc,
(4) Corner of 3rd lower slot of the dovetail-rim region of disc,
(5) Central part of disc,
(6) Bottom part of disc.

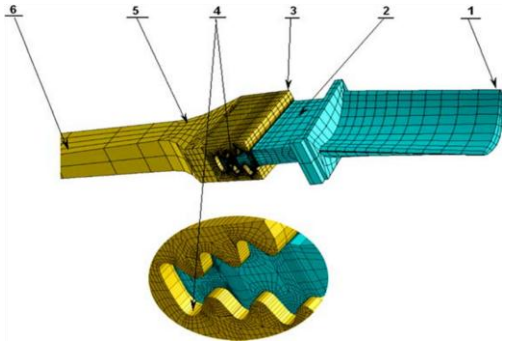

Fig.15
Specified control points of turbine blade.

The specified points were too useful to control the stresses and plastic strains of the turbine blade during its acceleration from 0 to 23,000 rpm.

6 CONCLUSIONS

In this study the fracture analysis was performed in order to investigate the damage mechanisms of the turbine disc and blade. The fractured blade, installed on the third stage rotor of the turbine of the turbojet engine, was initially cracked at the 6 cm distance from the hub of the blade by a fatigue mechanism over a period of time and then fractured instantly by the overload. The segregated area of Ti and Mo is found by the microstructure and EDX analysis of the blade. In order to solve this significant problem, a geometrically complicated FE model with some nonlinearities as contact and elastic–plastic material is also created. The analysis done for several conditions has indicated a few critical regions of the turbine, with operational and excessive rotational speed. The crack initiated at this area and was because of the stress concentration at the segregation of Mo and Ti nearby the blade surface. And this crack begins to progress. We proposed some useful suggestion such as:

1. Increase the radius of the lower slot of the serration fitting.
2. Change the dimensional tolerance of the dovetail-rim area of the turbine to unload the critical zone of the 3rd lower slot of the disc.
3. Proper manufacturing process (i.e., appropriate heat treatment)

Additional improvements of this paper are with the development and implementation of tools for alloy design, microstructure-process evolution, and mechanical-property modeling. Integration of the material-design and mechanical-design processes remains still an interesting challenge for future works.

REFERENCES

[1] Lucjan W., 2006, Failure analysis of turbine disc of an aero engine, *Engineering Failure Analysis* **13**: 9-17.

[2] Chan S.K., Tuba I.S., 1971, A finite element method for contact problems of solid bodies–Part II: Applications to turbine blade fastenings, *International Journal of Mechanical Sciences* **13**: 627-639.

[3] Masataka M., 1992, Root and groove contact analysis for steam turbine blades, *The Japan Society of Mechanical Engineers* **35**:508-514.

[4] Meguid S.A., Kanth P.S., Czekanski A., 2000, Finite element analysis of fir-tree region in turbine disc, *Finite Elements in Analysis and Design* **35**:305-317.

[5] Papanikos P., Meguid S.A., Stjepanovic Z., 1998, Three-dimensional nonlinear finite element analysis of dovetail joints in aero-engine discs, *Finite Elements in Analysis and Design* **29**:173-186.

[6] Zboinski G.,1995, Physical and geometrical non-linearities in contact problems of elastic turbine blade attachments, *International Journal of Mechanical Sciences* **209**: 273-286.

[7] McEvily A., 2004, Failures in inspection procedures: case studies, *Engineering Failure Analysis* **11**:167-176.

[8] Hou J., Wicks B.J., Antoniou R.A., 2002, An investigations of fatigue failures of turbine blades in a gas turbine engine by mechanical analysis, *Engineering Failure Analysis* **9**:201-211.

[9] Bhaumik S.K., 2002, Failure of turbine rotor blisk of an aircraft engine, *Engineering Failure Analysis* **9**: 287-301.

[10] Park M., Hwang Y., Choi Y., Kim T., 2002, Analysis of a J69-T-25 engine turbine blade fracture, *Engineering Failure Analysis* **9**: 593-601.

[11] Treager I., 1995, *Aircraft Gas Turbine Engine Technology*, McGraw Hill.

[12] Kyo-Soo S., Seon-Gab K., Daehan J., Young-Ha H., 2007, Analysis of the fracture of a turbine blade on a turbojet engine, *Engineering Failure Analysis* **14** : 877-883.

[13] Backman D. G., Mourer D. P., Bain K. R., Walston W. S., 2003, AIM- A new methodology for developing disk materials, *Advanced Materials and Processes for Gas Turbines* .

[14] Murakumo T., Kobayashi T., Koizumi Y., Harada H., 2004, Creep behavior of ni-base single-crystal super-alloys withvarious gamma volume fraction, *Acta Materialia* **52** (12): 3737-3744.

[15] Karunarante M. S. A., Reed R. C., 2003, Interdiffusion of platinum- group metals in nickel at elevated temperatures, *Acta Materialia* **51**(10): 2905-2914.

[16] Reed R. C., Karunarantne M. S. A., 2000, Interdiffusion in the face- centered cubic phase of Ni-Re, Ni-Ta and Ni-W systems between 900◦C and 1300◦C, *Materials Science and Engineering A* **281**(1–2): 229-233.

[17] WalstonW. S., Cetel A., MacKay R., O'Hara K., Duhl D., Dreshfield R., 2004, Joint development of a fourth generation single crystal super-alloys, *Super-Alloys* **2004**:15-24.

[18] Tanaka R., 2008, Research and development of ultra-high temperature materials in japan, *Materials at High Temperatures* **26**(4): 457-464.

[19] Pollock T. M., Argon A. S., 1992, Creep resistance of CMSX-3 nickel base super-alloys single crystals, *Acta Metallurgia et Materialia* **40**(6):1-30.

[20] McLean M., Dyson B. F., 2010, Modeling the effects of damage and microstructural evolution on the creep behavior of engineering alloys, *Journal of Engineering Materials and Technology* **131**:273-278.

[21] Pollock T. M., Field R. D., 2012, Dislocations and high temperature plastic deformation of super-alloys single crystals, *Dislocations in Solids* **2012**:549-618.
[22] *ASM Handbook*, ASM International **2**: 951.
[23] Meetham G.W.,1996, Contribution of materials to the development of the gas turbine engine, *Metall Mater Technology* **1996**: 589-602.
[24] Pollock T. M., Field R. D., 2002, Dislocations and high temperature plastic deformation of super-alloy single crystals, *Dislocations in Solids* **11**: 549-618.
[25] Rae C.M.F., Cox D.C., Rist M.A., Reed R.C., Matan N.C., 2000, On the primary creep of CMSX-4 super-alloy single crystals, *Metallurgical and Materials Transactions A* **31**(9): 2219-2228.
[26] Muller L., Glatzel U., Feller-Kniepmeier M., 1992, Modelling thermal misfit stresses in nickel-base super-alloys containing high volume fraction of gamma' phase, *Acta Metallurgia ET Materialia* **40**: 1321-1327.
[27] Schneider M. C., Gu J. P., Beckermann C., Boettinger W. J., Kattner U. R., 1997, Modeling of micro- and macros-egregation and freckle formation in single crystal nickel-base super-alloys during directional solidification, *Metallurgical Transactions A* **28**(7):1517-1531.
[28] Auburtin P., Cockcroft S. L., Mitchell A., 1996, Freckle formation in super-alloys, *Super-alloys* **1996**: 443-450.
[29] Miner R.V., Gayada J., Maier R.D., 1982, Fatigue and creep fatigue deformation of several nickel-base super-alloys at 650◦C, *Metallurgical Transactions A* 13(10):1755-1765.
[30] McLean M., Dyson B. F., 2000, Modeling the effects of damage and microstructural evolution on the creep behavior of engineering alloys, *Journal of Engineering Materials and Technology* **131**: 273-278.
[31] Carter Tim J., 2005, Common failures in gas turbine blade, *Engineering Failure Analysis* **12**: 237-247.
[32] *ASM Handbook*, ASM International **28**:50.
[33] Mercer C., Shademn S., Soboyejo W.O.,2003, An investigation of the micro-mechanisms of fatigue crack growth in structural gas turbine engine alloy, *Journal of Materials Science* **38**:291-305.
[34] Luo J., Bowen P., 2004, Small and long fatigue crack growth behavior of a PM Ni-based super-alloy, *International Journal of Fatigue* **26**:113-124.
[35] Jiang L., Brooks C.R., Liaw P.K., Klarstrom D.L., Rawn C.J., Muenchen B., 2001, Phenomenological aspects of the high-cycle fatigue of ULTIMET alloy, *Materials Science and Engineering* **316**:66-79.
[36] Neal D.F., Blenkinsop P.A., 1976, Internal fatigue origins in a–b titanium alloys, *Acta Metallurgica* **24**: 59-63.
[37] Boyd-Lee A.D., 1999, Fatigue crack growth resistant microstructures in polycrystalline Ni-base super-alloys for aeroengines, *International Journal of Fatigue* **21**:393-405.
[38] *MSC-Patran User's Manual*, 2009, MSC Corporation, Los Angeles.
[39] Park M., Hwang Y., Choi Y., Kim T., 2002, Analysis of a J69-T-25 engine turbine blade fracture, *Engineering Failure Analysis* **9**: 593-601.
[40] Pollock T.M., Tin S., 2006, Nickel-based supe-ralloys for advanced turbine engines: chemistry, microstructure, and properties , *Journal of Propulsion and Power* **22**(2): 361-374.
[41] Khurana S., Navte J., Singh H., 2012, Effect of cavitation on hydraulic turbines – a review, *International Journal of Current Engineering and Technology* **2**: 172 -177.
[42] Momcilvic D., Odanovic Z., Mitrovic R., Atanasovska I., Vuherer T., 2012, Failure analysis of hydraulic turbine shaft, *Engineering Failure Analysis* **29**: 54-66.
[43] Momcilovic D., Motrovic R., Antanasovska I., Vuherer T., 2012, Methodology of determination the influence of corrosion pit on the decrease of hydro turbine shaft fatigue failure, *Machine Design* **4**(4): 231 - 236.
[44] Neopane H.P., 2010, *Sediment Erosion in Hydro Turbines*, Faculty of Engineering Science and Technology, Fluid Engineering, Norway.
[45] Belash I., 2010, Causes of the failure of the no. 2 hydraulic generating set at the Sayano-Shushenskaya HPP: criticality of reliability enhancement for waterpower equipment, *Power Technology and Engineering* **44**(3):165-170.
[46] Ferreño D., Álvarez J.A., Ruiz E., Méndez D., Rodríguez L., Hernández D., 2011, Failure analysis of a Pelton turbine manufactured in soft martensitic stainless steel casting, *Engineering Failure Analysis* **18**(1):256-270.
[47] Egusquiza E., Valero C., Estévez A., Guardo A., Coussirat M., 2011, Failures due to ingested bodies in hydraulic turbines, *Engineering Failure Analysis* **18**(1): 464-473.
[48] Luo Y., Wang Z., Zeng J., Lin J., 2010, Fatigue of piston rod caused by unsteady, unbalanced, unsynchronized blade torques in a Kaplan turbine, *Engineering Failure Analysis* **17**(1):192-199.